Biochemistry and Biophysics Reports 4 (2015) 1–9

Contents lists available at ScienceDirect

Biochemistry and Biophysics Reports

journal homepage: www.elsevier.com/locate/bbrep

Cellulose nanocrystal cationic derivative induces NLRP3 inflammasome-dependent IL-1β secretion associated with mitochondrial ROS production

Rajesh Sunasee [a,*,1], Erinolaoluwa Araoye [a], Dejhy Pyram [a], Usha D. Hemraz [b,c], Yaman Boluk [c], Karina Ckless [a,*,2]

[a] Department of Chemistry, State University of New York at Plattsburgh, Hudson Hall, 101 Broad Street, Plattsburgh, NY, USA
[b] National Research Council of Canada, Montreal, Quebec, Canada
[c] Department of Civil & Environmental Engineering, University of Alberta and National Institute for Nanotechnology, National Research Council, Edmonton, Alberta, Canada

ARTICLE INFO

Article history:
Received 24 June 2015
Received in revised form
23 July 2015
Accepted 7 August 2015
Available online 14 August 2015

Keywords:
Cellulose nanocrystals
Cationic needle-like nanomaterial
NLRP3 inflammasome
IL-1β
Mitochondrial ROS
Mouse macrophages

ABSTRACT

Crystalline cellulose nanocrystals (CNCs) have emerged as novel materials for a wide variety of important applications such as nanofillers, nanocomposites, surface coatings, regenerative medicine and potential drug delivery. CNCs have a needle-like structure with sizes in the range of 100–200 nm long and 5–20 nm wide and a mean aspect ratio 10–100. Despite the great potential applicability of CNCs, very little is known about their potential immunogenicity. Needle-like materials have been known to evoke an immune response in particular to activate the (NOD-like receptor, pyrin domain-containing 3)-inflammasome/IL-1β (Interleukin 1β) pathway. In this study we evaluated the capacity of unmodified CNC and its cationic derivatives CNC-AEM (aminoethylmethacrylate)1, CNC-AEM2, CNC-AEMA(aminoethylmethacrylamide)1 and CNC-AEMA2 to stimulate NLRP3-inflammasome/IL-1β pathway and enhance the production of mitochondrial reactive oxygen species (ROS). Mouse macrophage cell line (J774A.1) was stimulated for 24 h with 50 μg/mL with unmodified CNC and its cationic derivatives. Alternatively, J774A1 or PBMCs (peripheral blood mononuclear cells) were stimulated with CNC-AEMA2 in presence or absence of LPS (lipopolysaccharide). IL-1β secretion was analyzed by ELISA, mitochondrial function by JC-1 staining and ATP content. Intracellular and mitochondrial reactive oxygen species (ROS) were assessed by DCF-DA (2′,7′-dichlorodihydrofluorescein diacetate) and MitoSOX, respectively. Mitochondrial ROS and extracellular ATP were significantly increased in cells treated with CNC-AEMA2, which correlates with the strongest effects on IL-1β secretion in non-primed cells. CNC-AEMA2 also induced IL-1βsecretion in LPS-primed and non-primed PBMCs. Our data suggest that the increases in mitochondrial ROS and ATP release induced by CNC-AEMA2 may be associated with its capability to evoke immune response. We demonstrate the first evidence that newly synthesized cationic cellulose nanocrystal derivative, CNC-AEMA2, has immunogenic properties, which may lead to the development of a potential non-toxic and safe nanomaterial to be used as a novel adjuvant for vaccines.

1. Introduction

Cellulose has a long history of use in the pharmaceutical industry because it has excellent compaction properties when blended with other pharmaceutical excipients, making this material suitable as a filler in tablets for oral administration of drugs [1,2]. In addition, its abundance, the relatively low cost and suitability for surface chemical modifications appeal to the pharmaceutical industry. In fact, modified cellulose has also been used extensively in pharmaceutical preparations, including ethyl cellulose, methyl cellulose, and carboxymethyl cellulose, in oral, topical, and injectable formulations [2]. Cellulose nanocrystals (CNCs) are a new renewable class of nanomaterials of great interest in industrial sectors. These elongated, rigid needle-like cellulose crystals (length, typically between 100 and 200 nm) obtained from

Abbreviations: AEM, aminoethylmethacrylate; AEMA, aminoethylmethacrylamide; ASC, apoptosis-associated speck-like protein containing a CARD; CNCs, cellulose nanocrystals; DAMPS, danger-associated molecular pattern molecules; DSL, Dynamic light scattering; ELISA, enzyme-linked immuno assay; H2DCF-DA, 2′, 7′-dichlorodihydrofluorescein diacetate; HRP, horseradish peroxidase-conjugated; HTCFNWs, high-temperature calcined fullerene nanowhiskers; IL-1β, Interleukin 1β; JC-1, 5,5′,6,6′-tetrachloro-1,1′,3,3′-tetraethylbenzimidazol-carbocyanine iodide; LPS, lipopolysaccharide; MWCNTs, needle-like multi-wall carbon nanotubes; NLRP3, NOD-like receptor, pyrin domain-containing 3; PAMPs, pathogen-associated molecular pattern molecules; PBMCs, peripheral blood mononuclear cells; ROS, reactive oxygen species; SAA, serum amyloid A; SDS-PAGE, sodium dodecyl sulfate polyacrylamide gel; TMB, 3,3′,5,5′ tetramethylbezidine

* Corresponding authors.
E-mail addresses: rsuna001@plattsburgh.edu (R. Sunasee), kckle001@plattsburgh.edu (K. Ckless).
[1] Tel.: +1 518 564 2703.
[2] Tel.: +1 518 564 4118.

http://dx.doi.org/10.1016/j.bbrep.2015.08.008

the acidic hydrolysis of native cellulose, display remarkable strength and physicochemical properties with several potential applications [3–6]. The ability to chemically modify CNCs through surface reactive hydroxyl groups opens up various potential applications otherwise unachievable with unmodified CNCs. Recently, CNCs have emerged as an interesting class of nanomaterials with potential biomedical applications mainly because some of their very desirable characteristics, such as nanoscale dimensions, biocompatibility, biodegradability and large surface area [7–10]. Although initial studies look promising, a great deal of work is still required to understand the integration of CNCs in the biological systems, in particular to evaluate the cytotoxicity and immunogenicity of these unmodified and modified CNCs. A recent *in vivo* study of the pulmonary toxicity of CNCs indicated that these nanomaterials can elicit dose-dependent oxidative stress, tissue damage, and inflammatory responses in the lungs [11]. However, the extent of the responses is highly dependent on the type of CNCs material. In fact, the needle-like morphology of CNCs could cause toxicity or immunogenicity, similar to carbonaceous fibers [12]. In addition, organic and inorganic particles (pollutants) have also been described as immunogenic because they activate the innate immune system *in vivo*. For instance, asbestos and silica induce NOD-like receptor, pyrin domain-containing 3 (NLRP3) inflammasome, leading to subsequent increases in the secretion of the pro-inflammatory cytokine Interleukin 1β (IL-1β) [13]. Another commonly used nanoparticle, nano-TiO(2) in biomedicine and electronic, activates the NLRP3 inflammasome, which ultimately leads to the release of IL-1β [14].

The IL-1 family of cytokines is critical to the host response to infection, playing a variety of roles not only in the acute phase response from the liver, but also in alterations of metabolism, induction of fever, and lymphocyte activation [15]. The two-step secretion of IL-1β requires the synthesis of several intracellular proteins, including pro-IL-1β and NLRP3, induced through a process known as “signal 1” or priming. The priming step can be accomplished by several stimuli from particles or “fibrin-like” molecules, microbial products called pathogen-associated molecular pattern molecules (PAMPs), to intracellular molecules released during death of neighboring cells, such as ATP and DNA, called danger-associated molecular pattern molecules (DAMPs) [16]. “Signal 2” is characterized by recruitment of the adapter protein apoptosis-associated speck-like protein containing a CARD (ASC) and pro-caspase-1, the latter of which becomes activated leading to the processing and secretion of IL-1β. Moreover, the cleavage and secretion of IL-1β can be enhanced by release of endogenous ATP that stimulates the purinergic receptor P2X7 [17]. It has been a consensus in the scientific literature that several identified NLRP3 activators also increase reactive oxygen species (ROS). It is well documented that activation of P2X7 is accompanied by production of intracellular ROS [13–18]. Initial studies using inhibitors supported a model in which ROS are generated by NADPH oxidases during NLRP3-inflammasome activation [19]. However, the idea that NADPH oxidases are the primary and solely source of ROS production during inflammasome activation is becoming less accepted. More recent studies indicated that increases in mitochondrial ROS and mitochondrial dysfunction also contribute to NLRP3 activation. In a previous study, we reported that serum amyloid A (SAA), a needle-like protein induces mitochondrial ROS and that uncoupling mitochondrial oxidative phosphorylation enhances NLRP3 activation by preventing the disassembly of NLRP3 complex [20]. Furthermore, other authors reported that oxidized mitochondrial DNA (mtDNA) when it is released into the cytosol can bind to and further activate the NLRP3 inflammasome [21].

In this study we evaluated the capacity of unmodified CNC and the cationic derivatives CNC-AEM1, CNC-AEM2, CNC-AEMA1 and CNC-AEMA2 to stimulate NLRP3-inflammasome/IL-1β axis and enhance the production of mitochondrial reactive oxygen species (ROS). Our main finding in this work is that only CNC-AEMA2 increases IL-1β secretion, and this effect correlates with the ability to increase both mitochondrial ROS and extracellular ATP in murine macrophage cell line. The other three cationic nanomaterials tested did not show any effect on the NLRP3 inflammasome IL-1β inflammatory pathway, and therefore they could be suitable for potential drug and gene delivery carriers.

2. Materials and methods

2.1. Chemicals and reagents

Sodium deoxycholate, 3,3′,5,5′ tetramethylbezidine (TMB), protease inhibitor cocktail, and anti β-actin antibody were purchased from Sigma. MitoTEMPO, the ROS detection reagent 2′,7′-dichlorodihydrofluorescein diacetate (H_2DCF-DA) and the mitochondrial ROS indicator (MitoSOX red), were purchased from Invitrogen. The mitochondrial membrane potential indicator, 5,5′,6,6′-tetrachloro-1,1′,3,3′-tetraethylbenzimidazol-carbocyanine iodide (JC-1) was purchased from Cayman. The ATP bioluminescence assay kit (StayBrite) was purchased from Biovision. NLRP3 antibody was purchased from Enzo, and antibodies for caspase-1 and IL-1β detection were purchased from Santa Cruz and Biovision, respectively. Secondary antibodies (anti-mouse horseradish peroxidase-conjugated (HRP) and anti-rabbit horseradish peroxidase-conjugated (HRP)) were obtained from GE Healthcare. IL-1β ELISA kits were purchased from BD Biosciences. *E. coli* 0111:B4 Lipopolysaccharide (LPS) was purchased from InvivoGen. Specific caspase 1 inhibitor yVAD was obtained from Calbiochem. lymphocyte separation medium (LSM) was obtained from MP Biomedicals. Freeze-dried unmodified CNC was obtained from Alberta Innovates Technology Futures (AITF), which was produced by a sulfuric acid mediated hydrolysis of cellulose [22]. The CNC cationic derivatives (CNC-AEM1, CNC-AEM2, CNC-AEMA1 and CNC-AEMA2) were synthesized using a radical cationic polymerization technique to produce brushes of methacrylate (AEM) or methacrylamide (AEMA) monomers on the CNCs surface. (Fig. 1). The difference between 1 and 2 is the molar ratio of monomers (AEM or AEMA) to anhydroglucose units, resulting in more or less cationic polymer brushes. Therefore both CNC-AEM1 and CNC-AEMA1 contain more brushes than CNC-AEM2 and CNC-AEMA2. The CNC-derivatives were extensively purified by centrifugation and dialysis to ensure efficient removal of unreacted reagents, monomers and homopolymers prior to all analyses. These CNC cationic derivatives were extensively characterized for their chemical and morphological features using a combination of analytical, spectroscopic, and microscopic techniques. Zeta potential measurements indicated a positive surface charge, and dynamic light scattering (DLS) was used to measure the size of the colloidal particles, which were found to be in the nanometer range (Table 1). Scanning transmission electron microscopy images revealed the size of the rod-like particles to be around 100–200 nm in length and 10–20 nm in diameter [23].

2.2. Cell culture and experimental conditions

Mouse monocyte (macrophage) cell line J774A.1 (obtained from ATCC) were seeded at 5×10^5 cells/mL using RPMI 1640 medium supplemented with 10% FBS, penicillin, streptomycin and L-glutamine, and incubated at 37 °C in a 5% CO_2-supplemented atmosphere for at least 24 h before the appropriate treatments. The blood cells were drawn from healthy donors and peripheral mononuclear cells (PBMCs) were isolated by centrifugation using

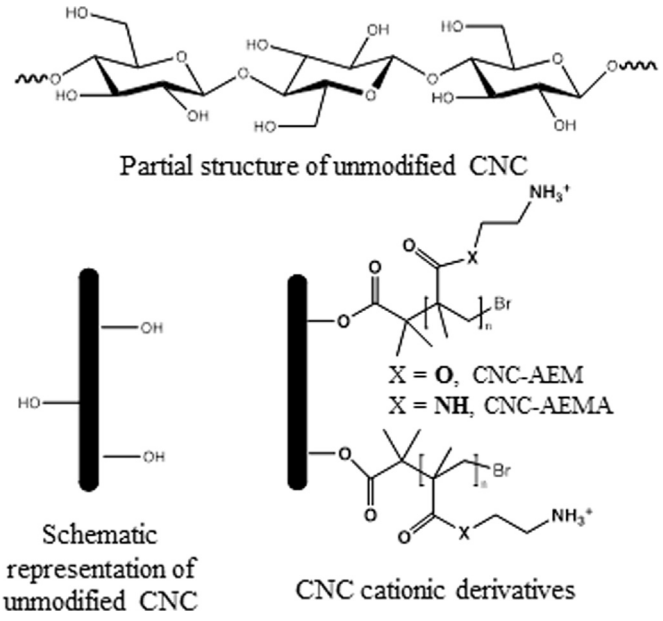

Fig. 1. Chemical structures of an unmodified CNC and CNC cationic derivatives used in this study.

Table 1
DLS and zeta potentials of cationic CNCs.

Sample	Size (nm)	Zeta potential (mV)
CNC-AEM1	161.6 ± 5.0	+56.4 ± 0.9
CNC-AEM2	154.6 ± 3.6	+45.2 ± 1.3
CNC-AEMA1	193.1 ± 4.6	+47.4 ± 4.6
CNC-AEMA2	183.4 ± 4.0	+43.9 ± 0.1

lymphocyte separation medium (LSM). The PBMCs were cultured for 24 h prior to stimulation. Unmodified CNC and CNC cationic derivatives (50 μg/mL) were utilized to stimulate J774A.1 cells at the indicated times. In this study we chose 50 μg/mL to perform all experiments, since in our previous work we demonstrated that J774A1 cells treated with CNC-AEMA2 (50 μg/mL) for 24 h, showed 93.5% of viable cells, indicating no significant cytotoxicity [23]. Alternatively, the cells were primed with 100 ng/mL of LPS and 6 h later different concentrations of CNC-AEMA2 were added, for a total of 24 h of treatment. The specific caspase 1 inhibitor, yVAD (10 μM) was added simultaneously to priming with LPS and 6 h later CNC-AEMA2 was added for another 18 h, completing the total of 24 h treatment. The antioxidant MitoTEMPO (50 μM) were added to stimulated cells at the indicated times.

2.3. Western blot analysis

After respective treatments, tissue culture plates were placed on ice and the attached cells were rinsed once with cold phosphate buffered saline (PBS) and lysed using lysis buffer (50 mM Tris, pH 7.4, 150 mM NaCl, 2 mM EDTA 0.2% Triton™ X-100, 0.3% IGEPAL® and protease inhibitor cocktail). The lysates were removed from the plate, transferred to microcentrifuge tubes and immediately frozen in liquid nitrogen to prevent protein degradation and enhance cell lysis. Cell lysates were equally loaded and proteins were separated on 10% sodium dodecyl sulfate polyacrylamide gels (SDS-PAGE) and transferred from the gel to a nitrocellulose membrane. The membrane was blocked for 1 h at RT with 3% milk in PBS containing 0.05% Tween®20 (PBST) and then incubated with respective antibodies overnight at 4 °C on a rotating platform. The membranes were washed 3 times PBST for 5 min each and incubated with respective HRP secondary antibodies. Western blots were developed utilizing 3,3′,5,5′ tetramethylbezidine (TMB) liquid substrate system for membranes according manufacturer's instructions.

2.4. Detection of IL-1β in cell supernatants and lysates

IL-1β secreted into the cell supernatants was quantified by Enzyme-linked immunoabsorbent assay (ELISA) according to the manufacturer's instruction [24]. For intracellular quantification of IL-β, cell lysates were prepared as described for Western blot analysis and ELISA performed following the manufacturer's protocol.

2.5. Detection of intracellular ROS

The H_2DCF-DA fluorescent assay was used to measure the presence of intracellular reactive oxygen species (ROS) [25]. Briefly, equal amount of cells (5×10^5 cells/mL) were seeded onto 8-well CultureSlides (BD Falcon™) and at 30 min prior to the end of treatments, 10 μM H_2DCF-DA in phenol red free DMEM media was added to the cells. The medium containing the fluorescent probes was removed, and the cells were rinsed with PBS, and observed in an Olympus BX53 fluorescence microscope coupled with Olympus DP73 digital camera. H_2O_2 (500 μM, 1 h) was added to the cells in medium containing 10% FBS. This oxidant is widely used as positive control for H_2DCF-DA fluorescent assay.

2.6. Detection of mitochondria-derived ROS

Mitochondria-derived ROS, was detected using the mitochondrial ROS indicator, MitoSOX red, a cationic dihydroethidium modified to target the mitochondria. MitoSOX red is a cell-permeable dye that reacts with superoxide to form ethidium, which upon binding to nucleic acids gives a bright red fluorescence. Briefly, equal amount of cells (5×10^5 cells/mL) were seeded onto 8-well CultureSlides (BD Falcon™) and at the end of the respective treatments rinsed with PBS and loaded with MitoSOX red (2.5 μM) for 10 min. The medium containing the fluorescent probes was removed, and the cells were rinsed with PBS, and observed in an Olympus BX53 fluorescence microscope coupled with Olympus DP73 digital camera.

2.7. Detection of mitochondrial membrane potential (Δψm)

Equal amount of cells (5×10^5 cells/mL) were seeded onto 8-well CultureSlides (BD Falcon™) and 24 h hours later treated as indicated. After washing with PBS, cells were incubated in fresh medium containing 5,5′,6,6′-tetrachloro-1,1′,3,3′-tetraethylbenzimidazol-carbocyanine iodide (JC-1) for 15 min. The dye was then removed; and cells were washed with PBS and fresh medium was added. Then live cells were immediately observed in an Olympus BX53 fluorescence microscope coupled with Olympus DP73 digital camera. Healthy cells, mainly JC-1 aggregates were observed at 540/570 nm excitation/emission and the apoptotic or unhealthy cells with mainly JC-1 monomers at 485/535 nm excitation/emission.

2.8. Measurement of ATP content

Assessment of ATP intracellular content was performed using the ATP bioluminescence assay kit following the manufacturer's instructions. In brief, after the respective treatment cells were lysated in 100 μL of lysis buffer (1% Triton™ X-100 in PBS) and 10 μL of the lysates were added to 90 μL of reaction buffer, which contains the enzyme mix. Alternatively, the extracellular ATP content was measured in cell culture supernatants by adding 10 μL of cell culture medium to 90 μL of reaction buffer. The luminescence was measured using a Synergy H1 Hybrid Multi-Mode Microplate Reader (BioTek). Values were expressed as relative fluorescence units (RLU).

2.9. Statistical analysis

The data were statistically analyzed by using the one-way analysis of variance test, followed by Bonferroni's multiple comparison test, using GraphPad Prizm 6 software.

3. Results

3.1. CNC cationic derivative induced IL-1β secretion and increased ROS production in mouse macrophages

We recently demonstrated that SAA, a needle-like protein considered a biomarker of inflammation, stimulated NLRP3 inflammasome-dependent IL-1β secretion in mouse peritoneal macrophages. Therefore, we sought to investigate whether or not unmodified CNC and its cationic derivatives would also induce NLRP3 inflammasome activation and IL-1β secretion in mouse macrophage cell line (J774A.1). Cells were stimulated with 50 μg/mL of unmodified CNC or CNC cationic derivatives for 24 h and cellular levels of inflammasome components were analyzed by Western blotting and IL-1β secretion was quantified by ELISA. Among the compounds tested, only CNC-AEMA2 induced significant IL-1β secretion, (Fig. 2A) and the AEMA polymer alone did not elicit IL-1β secretion in these cells, at the same experimental conditions (data not shown). In cells primed with lipopolysaccharide (LPS), this effect is enhanced and dose-dependent (Fig. 2B). Similar synergistic effects were also observed in human

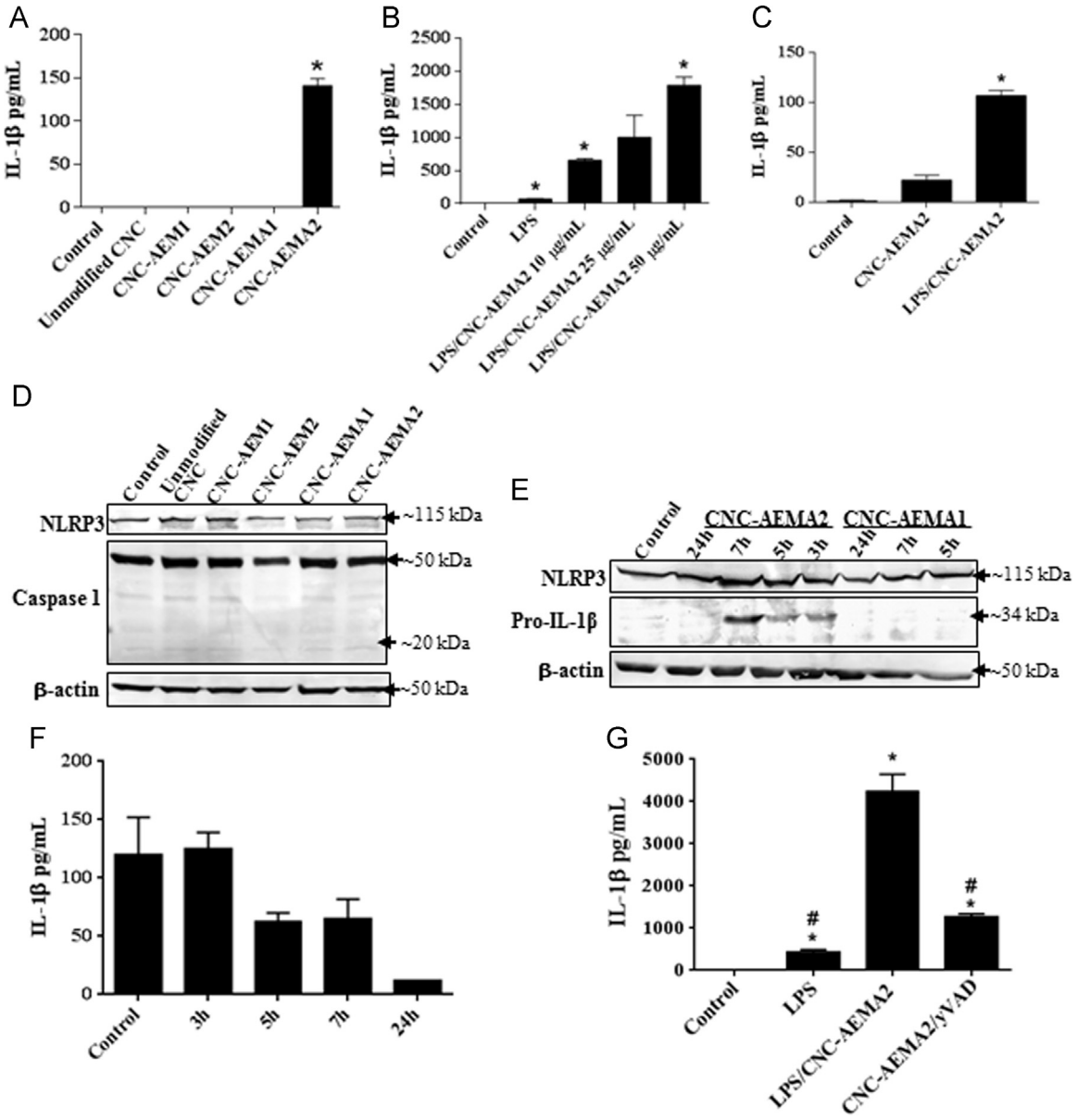

Fig. 2. Effect of unmodified CNC and its derivatives on NLRP3 inflammasome/IL-1β inflammatory pathway. J774A.1 mouse macrophage cell line were stimulated with unmodified CNC and its derivatives (50 μg/mL) for 24 h (A). Alternatively the cells were primed with 100 ng/mL of LPS and 6h later different concentrations of CNC-AEMA2 was added, for a total of 24 h of treatment (B). Human peripheral blood mononuclear cells (hPBMCs) were treated with CNC-AEMA2 alone or presence of LPS as described for J774A1 (C). Secreted IL-1β was quantified in the cell supernatants by ELISA (A, B, C). Data were means ± S.D. from triplicate. $^{*}p < 0.05$ compared to control. J774A.1 mouse macrophage cells were stimulated with unmodified CNC and its derivatives (50 μg/mL) for 24 h (D) or stimulated with CNC-AEMA1 or CNC-AEMA2 for the indicated times (E) and the intracellular NLRP3 inflammasome components were analyzed in the cells lysates by Western blotting. β-actin was used as loading control. Analysis of processed IL-1β in cell lysates from cells treated with 50 μg/mL of CNC-AEMA2 for the indicated times, was performed by ELISA (F). IL-1β secretion in primed cells was also investigated in presence of the caspase 1 inhibitor yVAD (10 μM), (G). $^{*}p < 0.05$ compared to control. $\#p < 0.05$ compared to LPS/CNC-AEMA2.

PMBCs (Fig. 2C). Surprisingly, upon 24 h of stimulation with unmodified CNC or CNC cationic derivatives no significant changes on the intracellular levels of NLRP3-inflammasome components, NLRP3, pro-IL1β (34 kDa) and pro- (50 kDa) or active caspase 1 (20 kDa) in comparison to non-stimulated cells (control) were observed (Fig. 2D). In addition, in control conditions J774A.1 cell line showed detectable levels of NLRP3, pro-caspase-1 (50 kDa) and no detectable pro-IL-1β (34 kDa). However, when the cells were stimulated with CNC-AEMA2 for a shorter period of time slight increase in the intracellular levels NLRP3 (Fig. 2E, top panel) and significant increase in pro-IL-1β (Fig. 2E, middle panel), were observed as early as 3 h and peaking at 7 h of incubation with CNC-AEMA2, but no detection of IL-1β release at these time points (data not shown). Since the Western blot analysis detects only pro-IL1β, we also investigated the intracellular levels of processed IL-1-β, using ELISA. Surprisingly, non-treated cells showed high level of intracellular IL-1β. The levels of IL-1β is reduced gradually as the time of incubation increases, and at 24 h of treatment we observed that the lowest intracellular level (Fig. 2F), coincides with the highest extracellular level of IL-1β (Fig. 2A). To confirm that caspase 1 is involved in the processing of pro-IL-1β into active and secreted form IL-1β in primed macrophages, the specific caspase 1 inhibitor (yVAD) was added to the cells concomitantly to LPS priming CNC-AEMA2. We observed that yVAD significantly decreases IL-1β secretion is CNC-AEMA2 treated cells upon LPS priming (Fig. 2G).

Since only CNC-AEMA2 was able to induce IL-1β secretion in our experimental conditions, we chose to utilize this CNC cationic derivative and its counterpart, CNC-AEMA1 to investigate further the mechanism by which this nanomaterial evokes immunogenic responses in mouse macrophage cell line. Augmented levels of ROS have been found as a common signal in NLRP3 inflammasome activation trigged by several activators [19–26]. Next we investigated the changes in the overall intracellular ROS levels in murine macrophages caused by stimulation with CNC cationic derivatives. H_2DCF-DA is a cell permeable fluorescence probe that is converted to the highly fluorescent 2′,7′-dichlorofluorescein (DCF). Although H_2DCF-DA can be oxidized to DCF by wide variety of reactive species [25–27], including by-products of its own oxidation [28], it is still a useful tool to investigate the overall oxidative status in biological system. We will utilize the term "intracellular ROS" as indicative of H_2DCF-DA oxidation caused by CNC cationic derivatives. As expected the basal level of intracellular ROS in non-stimulated cells (control) was found to be low and there was a subtle increase when cells were stimulated with CNC-AEMA2 (Fig. 3). The comparable control CNC-AEMA1 did not evoke significant increases in the intracellular ROS, under the experimental conditions tested. DCF fluorescence detects overall intracellular ROS, but not the source. Therefore, next we utilized a more specific fluorescent probe to detect mitochondrial ROS. MitoSOX red is designed to target mitochondria, where it undergoes oxidation by mitochondrial ROS and binds to nucleic acids, becoming highly fluorescent. Control cells showed low amount of mitochondrial ROS and surprisingly, both CNC-AEMA1 and CNC-AEMA2 elevated mitochondrial ROS in some extent. However, CNC-AEMA2 appears to be the most potent inducer of mitochondrial ROS (Fig. 4). Taken together, these data suggest that the NLRP3 inflammasome activation caused by CNC-AEMA2 stimulation is associated with increased and sustained intracellular and mitochondrial ROS production (detected at 24 h). Since we observed the increases in the intracellular NLRP3 inflammasome components occur at early time points of treatment (Fig. 2B) we decided to investigate whether this kinetic could also be observed in the intracellular and mitochondrial ROS production. Indeed CNC-AEMA2 induced temporal changes in both intracellular and mitochondrial ROS (Fig. 5A and B, respectively), and these changes, at 7 h of treatment with CNC-AEMA2 appears to correlate with induction of intracellular NLRP3 inflammasome components, such as pro-IL-1β.

3.2. Early mitochondrial ROS generation in NLRP3 inflammasome activation is involved in IL-1β secretion

It has been demonstrated that ROS scavengers or inhibitors added prior to or concomitant with NLRP3 stimulation diminish or abolish IL-1β secretion, implying a direct involvement of ROS in the NLRP3 inflammassome-IL-1β secretion axis [18,20,29]. Therefore, we utilized MitoTEMPO, a mitochondrial ROS scavenger, at different incubation times to investigate the impact of early and late mitochondrial ROS generation on NLRP3 inflammasome/IL-1β secretion in mouse macrophages. To investigate the early participation of mitochondrial ROS in this inflammatory pathway, we added MitoTEMPO concomitantly with CNC-AEMA2, and to analyze the late involvement of mitochondrial ROS in this pathway, we added it after 7 h of stimulation, when pro-IL-1β and NLRP3 are at their intracellular peak (Fig. 1C). We observed that when the cells were treated with CNC-AEMA2 concomitantly with MitoTEMPO, IL-1β secretion was significantly diminished when compared with CNC-AEMA2 alone. However, when MitoTEMPO was added 7 h after CNC-AEMA2 stimulation, its inhibitory effect was no longer observed (Fig. 6). As expected MitoTEMPO was capable to decrease mitochondrial ROS induced by CNC-AEMA2, regardless of time of incubation (Fig. 7), suggesting that early enhancing in mitochondrial ROS is associated with the increases in pro-IL-β

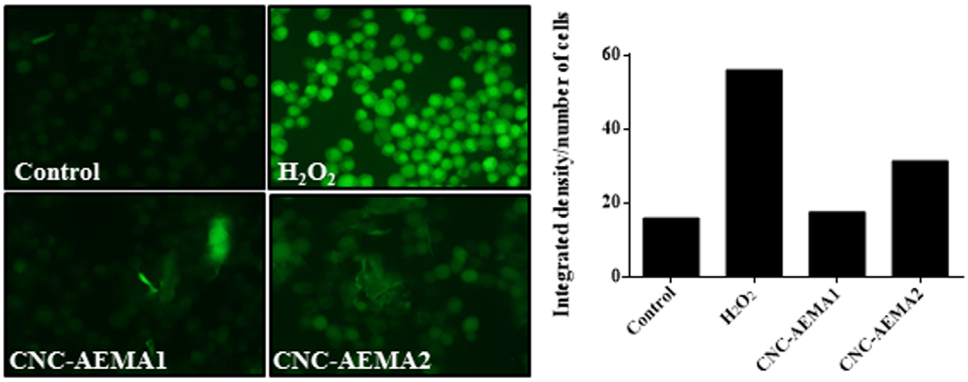

Fig. 3. Effect of CNC cationic derivatives on intracellular ROS. J774A.1 mouse macrophage cells were stimulated with CNC-AEMA1 or CNC AEMA2 (50 μg/mL) for 24 h or H_2O_2 (500 μM, 1 h positive control). After treatment, dihydrofluorescein diacetate (DCF-DA) was added to the live cells for 30 min and intracellular ROS levels from intact cells were analyzed utilizing a fluorescence microscope at 400 × magnification. The pixel intensity of each panel was analyzed using ImageJ and expressed as integrated intensity corrected by number of cell (graph on the right of the figure).

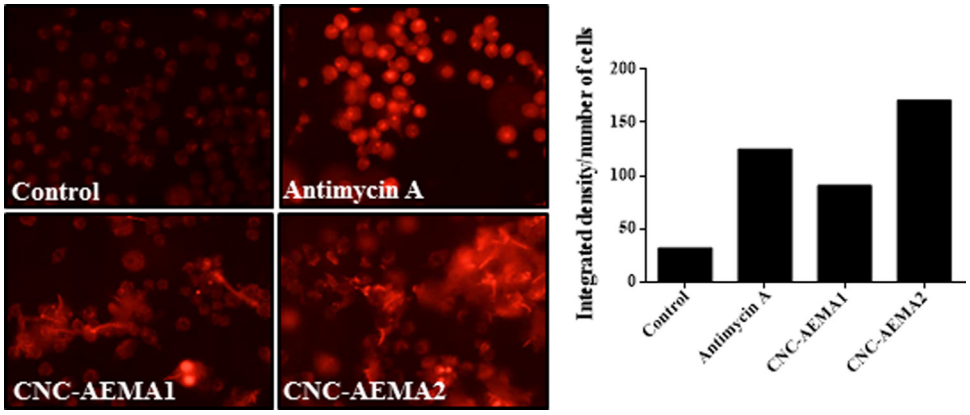

Fig. 4. Effect of CNC cationic derivatives on mitochondrial ROS. J774A.1 mouse macrophage cells were stimulated with CNC-AEMA1 or CNC-AEMA2 (50 μg/mL) for 24 h or Antimycin A (40 μg/mL, 3 h, mitochondrial ROS inducer, positive control). After treatment, MitoSOX red was added to the live cells for 10 min and mitochondrial ROS levels from intact cells were promptly analyzed utilizing a fluorescence microscope at 400 × magnification. The pixel intensity of each panel was analyzed using ImageJ and expressed as integrated intensity corrected by number of cell (graph on the right of the figure).

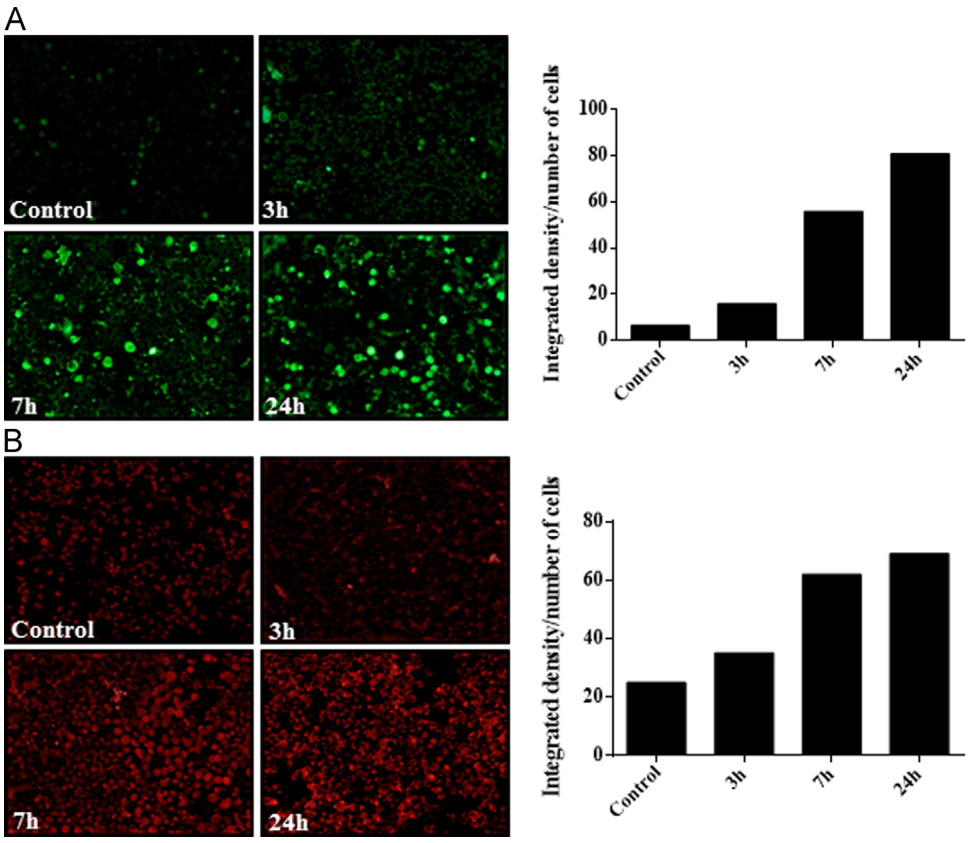

Fig. 5. Temporal changes in overall and mitochondrial ROS caused by CNC-AEMA2. J774A.1 mouse macrophage cells were stimulated with CNC-AEMA2 (50 μg/mL) at indicated times. After treatment, dihydrofluorescein diacetate (DCF-DA) or MitoSOX red was added to the live cells for 30 or 10 min, respectively and (A) intracellular ROS levels or (B) mitochondrial ROS levels both from intact cells were promptly analyzed utilizing a fluorescence microscope at 200 × magnification. The pixel intensity of each panel was analyzed using ImageJ and expressed as integrated intensity corrected by number of cell (graph on the right of the figure).

production, but not with the secretion in CNC-AEMA2-stimulated cells.

3.3. CNC cationic derivatives cause mitochondrial dysfunction

Several publications have implicated that dysfunctional mitochondria generates ROS, which ultimately sustain inflammasome activation and IL-1β secretion [20,30–32]. Since both CNC-AEMA1 and CNC-AEMAE2 demonstrated to increase mitochondrial ROS, we further investigated in more details the potential impact of these nanomaterials on the mitochondrial function. Mitochondrial dysfunction can be characterized by mitochondrial depolarization, mitochondrial permeabilization and energy depletion, therefore we assessed the impact of these drugs on mitochondrial membrane potential ($\Delta\Psi$), and ATP content. Mitochondrial depolarization was assessed by the widely used fluorescent probe JC-1, where green fluorescence indicates depolarized (monomer form of JC-1, unhealthy mitochondria) and red indicates hyperpolarized (J aggregate, healthy mitochondria). CNC-AEMA2 caused the most loss in mitochondrial membrane potential, indicated decreased in the red/green ratio, in comparison to untreated cells (Fig. 8). Depolarization of the mitochondrial membrane can have a direct impact on ATP production by the mitochondria.

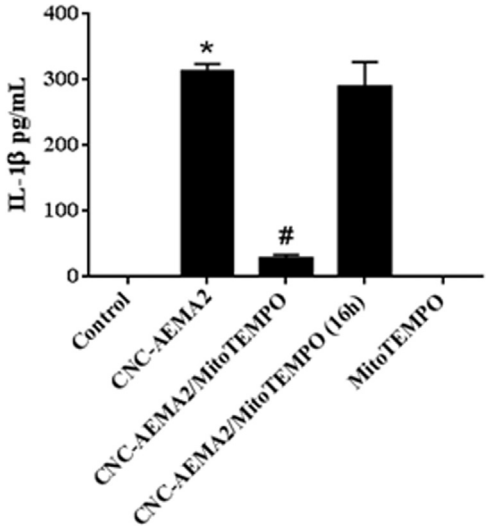

Fig. 6. Effects of mitochondrial ROS inhibitor, MitoTEMPO, on IL-1β secretion in cells stimulated with CNC-AEMA2. J774A.1 mouse macrophages were left to adhere for at least 24 h. The mitochondrial ROS scavenger, MitoTEMPO (10 μM) was added to the cells simultaneously to CNC-AEMA2 (50 μg/mL) stimulation. Alternatively cells were stimulated with CNC-AEMA2 (50 μg/mL) for 7 h, and then MitoTEMPO was added for another 16 h. After total 24 h of treatment IL-1β secretion was quantified by ELISA. The data are representative of at least two independent experiments performed in triplicates. $^{*}p < 0.05$ compared to control and $\#p < 0.05$ compared to CNC-AEMA2.

Therefore, we also measured intracellular and extracellular levels of ATP. Both CNC-AEMA1 and CNC-AEMA2 decreased intracellular ATP in J774A.1-treated cells, however CNC-AEMA2 has a more pronounced negative effect than CNC-AEMA1 (Fig. 9A), which is reflected on the significant increases in extracellular ATP content (Fig. 9B).

4. Discussion

In this study we report that a needle-like CNC cationic derivative, CNC-AEMA2, induces the secretion of proinflammatory cytokine IL-1β in mouse macrophage cell line (J774A.1), in absence of priming. It is important to mention that early studies demonstrating immunogenic activity of needle-like nanomaterials, such as amino-functionalized polystyrene [33] and carbon nanotubes [12] were performed in primed human macrophages. Our study provides the first evidence that early generation of mitochondrial-ROS are involved in the NLRP3 inflammasome activation and IL-1β secretion induced by this nanomaterial in non-primed J774A.1 cell line. The NLRP3 inflammasome/IL-1β inflammatory pathway is known to be activated by a variety of potential needle-like and particulate danger signals, including crystals of monosodium urate and cholesterol, silica crystals, aluminum salts, serum amyloid A (SAA) [20] in addition to bacterial toxins, oxidized mtDNA among others [26–34]. More recently, needle-like multi-wall carbon nanotubes (MWCNTs) and high-temperature calcined fullerene nanowhiskers (HTCFNWs) have been shown to induce NLRP3-mediated Il-1β secretion, in primed human macrophage cell line (THP-1) [35]. Although there is a consensus in the field that several "fiber/needle-like" molecules can elicit the NLRP3/IL-1β proinflammatory pathway, the mechanism by which this activation and consequent IL-1β secretion occurs remains to be elucidated. Variation in size, morphology and charge surface among these nanomaterials can enormously affect their biological activity [8,12,33]. For instance, when two different lengths of HTCFNWs (short 1.8 μm) and long (7.6 μm) were compared in their ability to induce NLRP3 inflammasome and IL-1β secretion in THP-1 cells, it was found that the long nanomaterial caused the greatest effect [35]. Our findings clearly demonstrated that CNC-AEMA2 was the only nanomaterial that was capable to induce secretion of IL-1β *in vitro*. We speculate that the combination of presence of amide instead of ester linkage (AEMA versus AEM) and the amount of brushes on the CNC surface (1, more brushes versus 2, less brushes) could have been the key factors for CNC-AEMA2 to elicit its pro-inflammatory effect. CNC-AEMA contains amide linkage, which is less electron dense than ester linkage found in CNC-AEM derivatives. This structural characteristic could facilitate CNC-AEMA2 to interact with cell membranes, since it could be less repulsed by the negatively charged membrane phospholipids. In addition, CNC-AEMA2 also contains fewer brushes than its count part nanomaterial CNC-AEMA1, and this feature could confer more capability to penetrate into the cells or cause disturbance on the cell membrane, and ultimately to induce IL-1β secretion [12]. However, it is still unclear whether CNC-AEMA2 in fact penetrates in the cell or stays on the cell surface.

An *in vivo* study analyzing the pulmonary toxicity of CNCs indicated that these nanomaterials can elicit dose-dependent oxidative stress, tissue damage, and inflammatory responses in the lungs [11]. We also observed that CNC-AEMA2 caused significant increases in intracellular and mitochondrial-ROS (Figs. 4 and 5B).

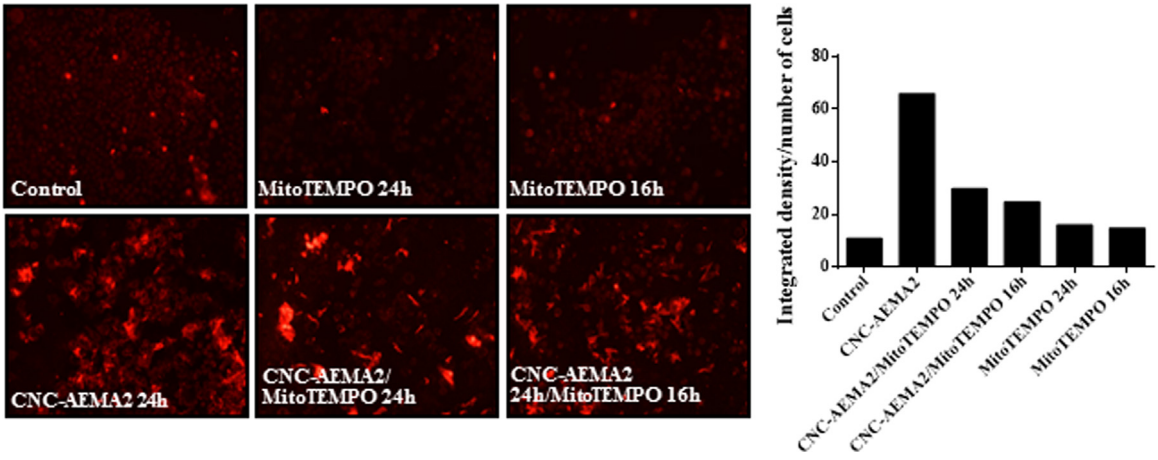

Fig. 7. Effect of CNC-AEMA2 on mitochondrial ROS. J774A.1 mouse macrophage cells were stimulated with CNC-AEMA2 (50 μg/mL) in presence or absence of MitoTEMPO (50 μM) for 24 h. Alternatively, cells were stimulated with CNC-AEMA2 (50 μg/mL) for 7 h, and then MitoTEMPO was added for another 16 h. After total 24 h of treatment, MitoSOX red was added to the live cells for 10 min and mitochondrial ROS levels from intact cells were promptly analyzed utilizing a fluorescence microscope at 200× magnification. The pixel intensity of each panel was analyzed using ImageJ and expressed as integrated intensity corrected by number of cell (graph on the right of the figure).

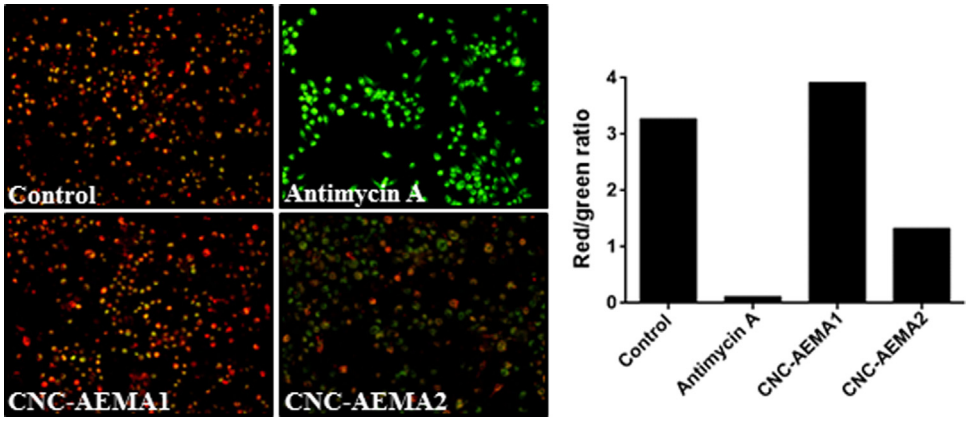

Fig. 8. Effect of CNC cationic derivatives on the mitochondrial membrane potential. J774A.1 mouse macrophage cells were stimulated with CNC-AEMA1 and CNC-AEMA2 (50 μg/mL) for 24 h or Antimycin A (40 μg/mL, 3 h, positive control). After treatment, JC-1 dye was added to the live cells for 10 min and mitochondrial membrane potential ($\Delta\psi m$) was promptly analyzed utilizing a fluorescence microscope at 200 × magnification. Green fluorescence indicates depolarized (monomer form of JC-1, unhealthy mitochondria) and red indicates hyperpolarized (J aggregate, healthy mitochondria). Consequently, dysfunctional mitochondria are indicated by a decrease in the red/green fluorescence intensity ratio (graph on the right of the figure). The red/green ratio was calculated using integrated intensity of red and green channels measured by ImageJ software.

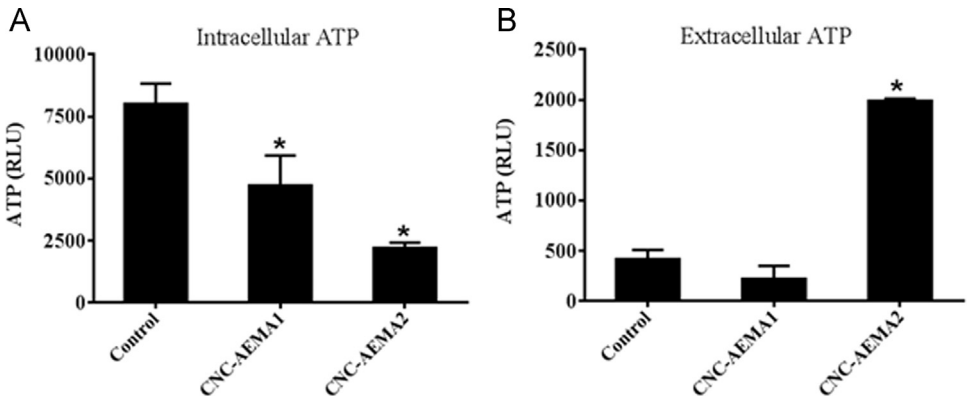

Fig. 9. Effect of CNC cationic derivatives on intracellular and extracellular ATP content. J774A.1 mouse macrophage cells were stimulated with CNC-AEMA1 or CNC-AEMA2 (50 μg/mL) for 24 h and after treatment ATP relative content in (A) cell lysates (intracellular ATP) and (B) supernatants (extracellular ATP) was analyzed with ATP bioluminescence assay kit. Data are expressed as relative luminescence units (RLU). Data were means ± S.D. from triplicate experiments. $^{*}p < 0.05$ compared to control.

This data is consistent with other findings in the literature indicating that activation of NLRP3 inflammasome is associated with increases in ROS production [26]. However, several studies suggest that the sources of increased ROS and the kinetics of this event is dependent on the nature of stimulation. We recently demonstrated that the increase in mitochondria-derived ROS in SAA-stimulated murine primary macrophages peaks as early as 2 h of stimulation and intracellular ROS at 24 h [20], which is somehow similar what was observed when mouse macrophages were stimulated with CNC-AEMA2 (Fig. 5A and B). In addition, in CNC-AEMA2 stimulated cells, the simultaneous treatment with mitochondrial antioxidant MitoTEMPO abolished the secretion of IL-1β. However, when MitoTEMPO was added post to 7 h of stimulation with CNC-AEMA2, the inhibitory effect on IL-1β secretion was no longer observed. This data suggested that the early increase in mitochondrial-derived ROS is directly related to synthesis of intracellular pro-IL1β but not to the secretion of IL-1β in CNC-AEMA2 stimulated cells. Several studies reinforce the idea that mitochondrial ROS, especially generated as a consequence of mitochondrial dysfunction, are the main source of ROS participating in NLRP3 inflammasome activation [20–31]. Although, it appears that CNC-AEMA2 action is mainly through mitochondrion, this compound was not the only one to cause mitochondrial alterations. CNC-AEMA1 was also able to mildly increase mitochondrial ROS. (Fig. 4). Analyzing mitochondria function we found that both CNC-AEMA1 and CNC-AEMA2 affected mitochondrial ROS production and intracellular ATP content, which is not surprisingly because these nanomaterials showed cationic nature [23] and it has also well known that other cationic molecules, such as cationic lipids [36] and amino functionalized polystyrene nanoparticles [33] can also cause mitochondrial dysfunction and activate NLRP3/IL-1β pathway. CNC-AEMA2 also caused some degree of changes in mitochondrial membrane potential, as seen with JC-1 mitochondrial staining (Fig. 8). However, the most striking observation is that CNC-AEMA2 significantly affects the extracellular levels of ATP (Fig. 9B). This dramatic augmentation on extracellular ATP could explain at least in part its action in increasing IL-1β secretion in CNC-AEMA2 treated cells. ATP is a well-known potent NLRP3 inflammasome post priming activator [26], and the secretion of IL-1β can largely be enhanced by increased concentration of extracellular ATP, which ultimately stimulates the purinergic receptor P2X7 [17]. It is important to mention that neither unmodified CNC or CNC cationic derivatives decreased cell viability in mouse macrophage cell line (J774A.1), under the experimental conditions tested [23].

5. Conclusion

In conclusion, our study indicates that the CNC cationic derivative, CNC-AEMA2 induced the secretion of the proinflammatory cytokine IL-1β in mouse macrophage, probably via a mechanism

involving increases in mitochondrial-derived ROS necessary for priming and consequent release of ATP to the extracellular environment, which causes IL-1β secretion. This data suggests that this cationic needle-like nanomaterial possesses immunogenic properties, and perhaps could be used as an adjuvant for vaccination, rather than as nanocarrier, as initially synthesized for [23]. In contrast, the other related CNC cationic derivatives did not show any immunogenic activity in our experimental conditions, and therefore they have potential applicability as drug and DNA delivery systems. However, because of the eminent biomedical applicability and potential large scale production of CNCs as well as CNC cationic derivatives, the biological effects and safety for human health of these nanomaterials must be thoroughly investigated *in vitro* before they can be used *in vivo*.

Acknowledgments

This work was supported by Presidential Award – SUNY Plattsburgh (2014–2015).

Appendix A. Suplementary information

Supplementary data associated with this article can be found in the online version at 10.1016/j.bbrep.2015.08.008.

References

[1] Susheel Kalia, Alain Dufresne, Bibin Mathew Cherian, B.S. Kaith, Luc Avérous, James Njuguna, E. Nassiopoulos, Nassiopoulos, cellulose-based bio- and nanocomposites: a review, Int. J. Polym. Sci. 2011 (2011) 35.
[2] J.K. Jackson, K. Letchford, B.Z. Wasserman, L. Ye, W.Y. Hamad, H.M. Burt, The use of nanocrystalline cellulose for the binding and controlled release of drugs, Int. J. Nanomed. 6 (2011) 321–330.
[3] Y. Habibi, L.A. Lucia, O.J. Rojas, Cellulose nanocrystals: chemistry, self-assembly, and applications, Chem. Rev. 110 (2010) 3479–3500.
[4] D. Klemm, F. Kramer, S. Moritz, T. Lindstrom, M. Ankerfors, D. Gray, A. Dorris, Nanocelluloses: a new family of nature-based materials, Angew. Chem. 50 (2011) 5438–5466.
[5] R.J. Moon, A. Martini, J. Nairn, J. Simonsen, J. Youngblood, Cellulose nanomaterials review: structure, properties and nanocomposites, Chem. Soc. Rev. 40 (2011) 3941–3994.
[6] B.L. Peng, N. Dhar, H.L. Liu, K.C. Tam, Chemistry and applications of nanocrystalline cellulose and its derivatives: A nanotechnology perspective, Can. J. Chem. Eng. 89 (2011) 15.
[7] S. Dong, M. Roman, Fluorescently labeled cellulose nanocrystals for bioimaging applications, J. Am. Chem. Soc. 129 (2007) 13810–13811.
[8] K.A. Mahmoud, J.A. Mena, K.B. Male, S. Hrapovic, A. Kamen, J.H. Luong, Effect of surface charge on the cellular uptake and cytotoxicity of fluorescent labeled cellulose nanocrystals, ACS Appl. Mater. Interfaces 2 (2010) 2924–2932.
[9] T. Kovacs, V. Naish, B. O'Connor, C. Blaise, F. Gagne, L. Hall, V. Trudeau, P. Martel, An ecotoxicological characterization of nanocrystalline cellulose (NCC), Nanotoxicology 4 (2010) 255–270.
[10] E. Lam, K.B. Male, J.H. Chong, A.C. Leung, J.H. Luong, Applications of functionalized and nanoparticle-modified nanocrystalline cellulose, Trends Biotechnol. 30 (2012) 283–290.
[11] N. Yanamala, M.T. Farcas, M.K. Hatfield, E.R. Kisin, V.E. Kagan, C.L. Geraci, A. A. Shvedova, In vivo evaluation of the pulmonary toxicity of cellulose nanocrystals: a renewable and sustainable nanomaterial of the future, ACS Sustain. Chem. Eng. 2 (2014) 1691–1698.
[12] J. Palomaki, E. Valimaki, J. Sund, M. Vippola, P.A. Clausen, K.A. Jensen, K. Savolainen, S. Matikainen, H. Alenius, Long, needle-like carbon nanotubes and asbestos activate the NLRP3 inflammasome through a similar mechanism, ACS Nano 5 (2011) 6861–6870.
[13] C. Dostert, V. Petrilli, R. Van Bruggen, C. Steele, B.T. Mossman, J. Tschopp, Innate immune activation through Nalp3 inflammasome sensing of asbestos and silica, Science 320 (2008) 674–677.
[14] A.S. Yazdi, G. Guarda, N. Riteau, S.K. Drexler, A. Tardivel, I. Couillin, J. Tschopp, Nanoparticles activate the NLR pyrin domain containing 3 (Nlrp3) inflammasome and cause pulmonary inflammation through release of IL-1{alpha} and IL-1{beta}, Proc. Natl. Acad. Sci. USA 104 (2010) 19449–19454.
[15] C.A. Dinarello, Immunological and inflammatory functions of the interleukin-1 family, Annu. Rev. Immunol. 27 (2009) 519–550.
[16] F. Martinon, A. Mayor, J. Tschopp, The inflammasomes: guardians of the body, Annu. Rev. Immunol. 27 (2009) 229–265.
[17] A. Piccini, S. Carta, S. Tassi, D. Lasiglie, G. Fossati, A. Rubartelli, ATP is released by monocytes stimulated with pathogen-sensing receptor ligands and induces IL-1beta and IL-18 secretion in an autocrine way, Proc. Natl. Acad. Sci. USA 105 (2008) 8067–8072.
[18] C.M. Cruz, A. Rinna, H.J. Forman, A.L. Ventura, P.M. Persechini, D.M. Ojcius, ATP activates a reactive oxygen species-dependent oxidative stress response and secretion of proinflammatory cytokines in macrophages, J. Biol. Chem. 282 (2007) 2871–2879.
[19] F. Martinon, Signaling by ROS drives inflammasome activation, Eur. J. Immunol. 40 (2010) 616–619.
[20] J. Jabaut, J.L. Ather, A. Taracanova, M.E. Poynter, K. Ckless, Mitochondria-targeted drugs enhance Nlrp3 inflammasome-dependent IL-1beta secretion in association with alterations in cellular redox and energy status, Free Radic. Biol. Med. 60 (2013) 233–245.
[21] K. Shimada, T.R. Crother, J. Karlin, J. Dagvadorj, N. Chiba, S. Chen, V. K. Ramanujan, A.J. Wolf, L. Vergnes, D.M. Ojcius, A. Rentsendorj, M. Vargas, C. Guerrero, Y. Wang, K.A. Fitzgerald, D.M. Underhill, T. Town, M. Arditi, Oxidized mitochondrial DNA activates the NLRP3 inflammasome during apoptosis, Immunity 36 (2012) 401–414.
[22] Y. Boluk, R. Lahiji, L. Zhao, M.T. McDermott, Suspension viscosities and shape parameter of cellulose nanocrystals (CNC), Colloids Surf. 377 (2011) 297–303.
[23] U.D. Hemraz, K.A. Campbell, J.S. Burdick, K. Ckless, Y. Boluk, R. Sunasee, Cationic poly(2-aminoethylmethacrylate) and poly(N-(2-aminoethylmethacrylamide) modified cellulose nanocrystals: synthesis, characterization, and cytotoxicity, Biomacromolecules 16 (2015) 319–325.
[24] J.L. Ather, K. Ckless, R. Martin, K.L. Foley, B.T. Suratt, J.E. Boyson, K.A. Fitzgerald, R.A. Flavell, S.C. Eisenbarth, M.E. Poynter, Serum amyloid a activates the NLRP3 Inflammasome and promotes Th17 allergic asthma in mice, J. Immunol. 187 (2011) 64–73.
[25] O. Myhre, J.M. Andersen, H. Aarnes, F. Fonnum, Evaluation of the probes 2′,7′-dichlorofluorescin diacetate, luminol, and lucigenin as indicators of reactive species formation, Biochem. Pharmacol. 65 (2003) 1575–1582.
[26] O. Gross, C.J. Thomas, G. Guarda, J. Tschopp, The inflammasome: an integrated view, Immunol. Rev. 243 (2011) 136–151.
[27] P. Bilski, A.G. Belanger, C.F. Chignell, Photosensitized oxidation of 2′,7′-dichlorofluorescin: singlet oxygen does not contribute to the formation of fluorescent oxidation product 2′,7′-dichlorofluorescein, Free Radic. Biol. Med. 33 (2002) 938–946.
[28] M.G. Bonini, C. Rota, A. Tomasi, R.P. Mason, The oxidation of 2′,7′-dichlorofluorescin to reactive oxygen species: a self-fulfilling prophesy? Free Radic. Biol. Med. 40 (2006) 968–975.
[29] S. Tassi, S. Carta, L. Delfino, R. Caorsi, A. Martini, M. Gattorno, A. Rubartelli, Altered redox state of monocytes from cryopyrin-associated periodic syndromes causes accelerated IL-1beta secretion, Proc. Natl. Acad. Sci. USA 107 (2010) 9789–9794.
[30] A.C. Bulua, A. Simon, R. Maddipati, M. Pelletier, H. Park, K.Y. Kim, M.N. Sack, D. L. Kastner, R.M. Siegel, Mitochondrial reactive oxygen species promote production of proinflammatory cytokines and are elevated in TNFR1-associated periodic syndrome (TRAP), J. Exp. Med. 208 (2011) 519–533.
[31] J. Tschopp, Mitochondria: sovereign of inflammation? Eur. J. Immunol. 41 (2011) 1196–1202.
[32] R. Zhou, A.S. Yazdi, P. Menu, J. Tschopp, A role for mitochondria in NLRP3 inflammasome activation, Nature 469 (2011) 221–225.
[33] O. Lunov, T. Syrovets, C. Loos, G.U. Nienhaus, V. Mailander, K. Landfester, M. Rouis, T. Simmet, Amino-functionalized polystyrene nanoparticles activate the NLRP3 inflammasome in human macrophages, ACS Nano 5 (2011) 9648–9657.
[34] J. Henao-Mejia, E. Elinav, T. Strowig, R.A. Flavell, Inflammasomes: far beyond inflammation, Nat. Immunol. 13 (2012) 321–324.
[35] H. Cui, W. Wu, K. Okuhira, K. Miyazawa, T. Hattori, K. Sai, M. Naito, K. Suzuki, T. Nishimura, Y. Sakamoto, A. Ogata, T. Maeno, A. Inomata, D. Nakae, A. Hirose, T. Nishimaki-Mogami, High-temperature calcined fullerene nanowhiskers as well as long needle-like multi-wall carbon nanotubes have abilities to induce NLRP3-mediated IL-1beta secretion, Biochem. Biophys. Res. Commun. 452 (2014) 593–599.
[36] C. Lonez, M. Bessodes, D. Scherman, M. Vandenbranden, V. Escriou, J. M. Ruysschaert, Cationic lipid nanocarriers activate toll-like receptor 2 and NLRP3 inflammasome pathways, Nanomed. Nanotechnol. Biol. Med. 10 (2014) 775–782.